Systems/Circuits

Fine Control of Sound Frequency Tuning and Frequency Discrimination Acuity by Synaptic Zinc Signaling in Mouse Auditory Cortex

Manoj Kumar,[1] **Shanshan Xiong,**[1,2] **Thanos Tzounopoulos,**[1] **and Charles T. Anderson**[1]

[1]Pittsburgh Hearing Research Center and Department of Otolaryngology, University of Pittsburgh, Pittsburgh, Pennsylvania 15261 and [2]The Third Xiangya Hospital, Central South University, Changsha, China 410013

Neurons in the auditory cortex are tuned to specific ranges of sound frequencies. Although the cellular and network mechanisms underlying neuronal sound frequency selectivity are well studied and reflect the interplay of thalamocortical and intracortical excitatory inputs and further refinement by cortical inhibition, the precise synaptic signaling mechanisms remain less understood. To gain further understanding on these mechanisms and their effects on sound-driven behavior, we used *in vivo* imaging as well as behavioral approaches in awake and behaving female and male mice. We discovered that synaptic zinc, a modulator of neurotransmission and responsiveness to sound, sharpened the sound frequency tuning of principal and parvalbumin-expressing neurons and widened the sound frequency tuning of somatostatin-expressing inhibitory neurons in layer 2/3 of the primary auditory cortex. In the absence of cortical synaptic zinc, mice exhibited reduced acuity for detecting changes in sound frequencies. Together, our results reveal that cell-type-specific effects of zinc contribute to cortical sound frequency tuning and enhance acuity for sound frequency discrimination.

Key words: **auditory cortex; cortical tuning; neuromodulation; sensory processing; synaptic signaling; synaptic zinc**

Significance Statement

Neuronal tuning to specific features of sensory stimuli is a fundamental property of cortical sensory processing that advantageously supports behavior. Despite the established roles of synaptic thalamocortical and intracortical excitation and inhibition in cortical tuning, the precise synaptic signaling mechanisms remain unknown. Here, we investigated these mechanisms in the mouse auditory cortex. We discovered a previously unknown signaling mechanism linking synaptic zinc signaling with cell-specific cortical tuning and enhancement in sound frequency discrimination acuity. Given the abundance of synaptic zinc in all sensory cortices, this newly discovered interaction between synaptic zinc and cortical tuning can provide a general mechanism for modulating neuronal stimulus specificity and sensory-driven behavior.

Introduction

In the sensory cortex, cortical neurons respond to specific features of the sensory stimulus. This is a dominant property of sensory processing that advantageously supports behavior. Therefore, elucidating the neuronal mechanisms underlying sensory stimulus selectivity is crucial for understanding how the brain encodes sensory information to guide behavior. Here, we investigated these mechanisms in the mouse auditory cortex as well as their effect on sound frequency discrimination acuity.

In the mouse auditory cortex, cortical neurons are tuned to ranges of sound frequencies (Merzenich et al., 1973; Bizley et al., 2005; Bandyopadhyay et al., 2010; Guo et al., 2012; Moore and Wehr, 2013). In the auditory and other sensory cortices, this tuning is shaped by tuned thalamocortical input (L.Y. Li et al., 2013) as well as the interaction of excitatory and inhibitory intracortical inputs, with cortical inhibition playing a crucial role in refining stimulus selectivity (Priebe and Ferster, 2008; Isaacson and Scanziani, 2011). Whereas previous studies have established the role of synaptic excitation and inhibition on sound frequency tuning, the modulatory signaling mechanisms that fine-tune cortical specificity to sound frequencies are not well understood. To

Received May 25, 2018; revised Oct. 16, 2018; accepted Nov. 16, 2018.

Author contributions: M.K., T.T., and C.T.A. designed research; M.K., S.X., and C.T.A. performed research; M.K., S.X., and C.T.A. analyzed data; M.K., T.T., and C.T.A. wrote the paper.

This work was supported by NIH Grant R01-DC007905 (to T.T.) and National Science Foundation Grant IOS-1655480 (to T.T.). We thank Drs. Brent Doiron and Amantha Thathiah for their critical reading and helpful comments on this manuscript. We acknowledge Drs. Vivek Jayaraman, Douglas S. Kim, Loren L. Looger, and Karel Svoboda from the GENIE Project (Janelia Research Campus, Howard Hughes Medical Institute) for making GCaMP6f available.

The authors declare no competing financial interests.

Correspondence should be addressed to Thanos Tzounopoulos at thanos@pitt.edu or Charles T. Anderson at charles.anderson@hsc.wvu.edu.

https://doi.org/10.1523/JNEUROSCI.1339-18.2018

 0270-6474/19/390854-12$15.00/0

address this question, we studied the role of synaptic zinc in shaping cortical frequency tuning and in modulating sound frequency discrimination acuity.

In many brain areas, including the sensory neocortex, hippocampus, and amygdala, synaptic zinc is released from glutamatergic vesicles to fine-tune neurotransmission by mostly modulating AMPA receptor (AMPAR) and NMDA receptor (NMDAR) EPSCs as well as presynaptic probability of release (Vogt et al., 2000; Pan et al., 2011; Perez-Rosello et al., 2013; Vergnano et al., 2014; Anderson et al., 2015; Kalappa et al., 2015; Kalappa and Tzounopoulos, 2017). In the auditory cortex, synaptic zinc has recently emerged as a novel modulator of sound processing that increases the gain of sound-evoked responses in layer 2/3 principal neurons by reducing the gain of parvalbumin (PV)- and somatostatin (SOM)-expressing neurons (Anderson et al., 2017; McAllister and Dyck, 2017). Here, we tested whether synaptic zinc shapes cortical frequency tuning and sound frequency discrimination.

To answer this question, we used *in vivo* two-photon calcium imaging of specific neuronal types to test the effects of synaptic zinc signaling on frequency tuning. Moreover, we used behavioral paradigms to assess the role of synaptic zinc on sound frequency discrimination. Our results highlight synaptic zinc as a novel modulator of cortical frequency tuning. In the absence of cortical synaptic zinc, altered tuning of auditory processing results in reduced acuity in sound frequency discrimination.

Materials and Methods

Animals. All procedures were approved by the Institutional Animal Care and Use Committee at the University of Pittsburgh. Male and female ICR mice (The Jackson Laboratory) were used for the experiments shown in Figure 1*a–m* (AAV-CaMKII-GCaMP6f) and Figure 5*b–e*. Male and female ZnT3 KO mice, which lack the vesicular zinc transporter ZnT3 and thus synaptic zinc (Cole et al., 1999; The Jackson Laboratory), were used for the experiments shown in Figures 1*n–p*, 4*b–i*, and 5*f*. Male and female ZnT3 WT mice were used for the experiments shown in Figure 4*b–i*. Male and female PV-Cre mice (The Jackson Laboratory) were used for the experiments shown in Figure 2. Male and female SOM-Cre mice (The Jackson Laboratory) were used for the experiments shown in Figure 3.

Adeno-associated virus injections for in vivo *imaging.* Male or female ICR mice (The Jackson Laboratory), ZnT3 KO mice (The Jackson Laboratory), PV-Cre mice, and SOM-Cre mice (The Jackson Laboratory) were anesthetized with inhaled isoflurane (induction, 3% in oxygen; maintenance, 1.5% in oxygen) and secured in a stereotaxic frame (Kopf). Mice were between postnatal day 19 (P19) and P36. Core body temperature was maintained at ~37°C with a heating pad, and eyes were protected with ophthalmic ointment. Lidocaine (1%) was injected under the scalp, and an incision was made into the skin at the midline to expose the skull. Using a 27 gauge needle as a scalpel, a small craniotomy (~0.4 mm diameter) was made over the right temporal cortex (~4 mm lateral to lambda). A glass micropipette, containing adeno-associated virus (AAV) vectors, driven by CaMKII or Flex promoters for neuron-specific expression, was inserted into the cortex 0.5–1 mm past the surface of the skull with a micromanipulator (Kopf). We used AAV9.CaMKII.GCaMP6f.WPRE.SV40 and AAV9.CAG.Flex.GCaMP6f.WPRE.SV40 (titer $5e^{12}$–$5e^{13}$ genome copies per milliliter, Penn Vector Core; Chen et al., 2013). The glass micropipette was backfilled with mineral oil and connected to a 5 μl glass syringe (Hamilton). We used a syringe pump (World Precision Instruments) to inject 200–400 nl of this solution over the course of 5 min. The pipette was left in place for 2 min after the end of the injection. The pipette was then removed, and the scalp of the mouse was closed with cyanoacrylate adhesive. Mice were fed a diet containing the nonsteroidal anti-inflammatory drug carprofen (Medigel) for 24 h before and 48 h after surgery. Mice were monitored for signs of postoperative stress and pain.

In vivo *imaging.* Eleven to 24 days after AAV injections, mice were prepared for *in vivo* calcium imaging. Mice were anesthetized with inhaled isoflurane (induction, 3% in oxygen; maintenance, 1.5% in oxygen) and positioned into a custom-made head holder. Core body temperature was maintained at ~37°C with a heating pad, and eyes were protected with ophthalmic ointment. Lidocaine (1%) was injected under the scalp, and an incision (~1.5 cm long) was made into the skin over the right temporal cortex. The head of the mouse was rotated ~45° in the coronal plane to align the pial surface of the right temporal cortex with the imaging plane of the upright microscope optics. The skull of the mouse was secured to the head holder using dental acrylic (Lang) and cyanoacrylate adhesive. A tube (the barrel of a 25 ml syringe or an SM1 tube from Thorlabs) was placed around the animal's body to reduce movement, and the mouse received an injection of the sedative chlorprothixene (0.36 mg/kg, i.m.) to reduce animal movement during *in vivo* imaging (Chen et al., 2013; Kato et al., 2015). A dental acrylic reservoir was created to hold warm (37°C) ACSF over the exposed skull. In preparing the ACSF, we removed contaminating zinc by incubating with Chelex 100 resin (BioRad) for 1 h. Subsequently, we removed the Chelex by vacuum filtration and added high-purity calcium and magnesium salts (99.995% purity; Sigma-Aldrich). The solution contained (in mM) 130 NaCl, 3 KCl, 2.4 $CaCl_2$, 1.3 $MgCl_2$, 20 $NaHCO_3$, 3 HEPES, and 10 D-glucose, pH 7.25–7.35, ~300 mOsm. For better optical access of the auditory cortex, we injected lidocaine–epinephrine (2% lidocaine, 1:100,000 w/v epinephrine) into the temporal muscle and retracted a small portion of the muscle from the skull. Mice were then positioned under the microscope objective in a sound- and light-attenuation chamber containing the microscope and a calibrated speaker (ES1, Tucker-Davis). Acoustic stimuli were calibrated with a free-field, compensated ¼ inch microphone (4954-B, Bruel & Kjar) placed at the location of the animal's ear within the chamber.

Transcranial imaging. We performed transcranial imaging to locate the primary auditory cortex (A1) in each mouse (Fig. 1*a*,*b*). We removed the isoflurane from the oxygen flowing to the animal and began imaging sound-evoked responses at least 10 min later (Issa et al., 2014; Anderson et al., 2015). Sounds were delivered from a free-field speaker 10 cm from the left ear of the animal (ES1 speaker, ED1 driver, Tucker-Davis Technologies), controlled by a digital-to-analog converter with an output rate of 250 kHz (USB-6229, National Instruments). We used ephus (Suter et al., 2010) to generate the sound waveforms and synchronize the sound delivery and image acquisition hardware. We presented 50 or 60 dB SPL, 6 kHz tones to the animal while illuminating the skull with a blue LED (nominal wavelength, 490 nm; M490L2, Thorlabs). We imaged the change in green GCaMP6f emission with epifluorescence optics (eGFP filter set, U-N41017, Olympus) and a 4× objective (Olympus) using a cooled CCD camera (Rolera, Q-Imaging). Images were acquired at a resolution of 174 × 130 pixels (using 4× spatial binning, each pixel covered an area of 171.1 μm^2 of the image) at a frame rate of 20 Hz to locate A1 in each animal (see below, Analysis).

Transcranial imaging analyis. To localize A1, we used 50 or 60 dB SPL, 6 kHz tones, and we normalized the sound-evoked change in fluorescence after sound presentation (ΔF) to the baseline fluorescence (F), where F is the average fluorescence of 1 s preceding the sound onset (for each pixel in the movie). We applied a two-dimensional, low-pass Butterworth filter to each frame of the $\Delta F/F$ movie and created an image consisting of a temporal average of 10 consecutive frames (0.5 s) beginning at the end of the sound stimulus. This image indicated two sound-responsive regions corresponding to the low-frequency tonotopic areas of A1 and the anterior auditory field (AAF; Fig. 1*b*).

Two-photon imaging. For two-photon imaging in awake mice, after locating A1 as described above, we reanesthetized the mouse with isoflurane and created a craniotomy (~1 mm^2) over A1 for improved optical access (Fig. 1*c*). Using a micromanipulator (Siskiyou), we inserted a glass micropipette backfilled with mineral oil and connected to a 5 μl glass syringe into the cortex at the edge of this craniotomy (Fig. 1*c*). The pipette contained ACSF including 100 μM ZX1 (Pan et al., 2011; Anderson et al., 2015; an extracellular, high-affinity, fast, zinc-specific chelator) and 50 μM Alexa Fluor 594. Once the pipette was inserted into the cortex, we removed the isoflurane and began two-photon imaging after 20 min

of recovery from isoflurane. Mode-locked infrared laser light (940 nm, 100–200 mW intensity at the back focal plane of the objective, MaiTai HP, Newport) was delivered through a galvanometer-based scanning two-photon microscope (Scientifica) controlled with ScanImage 3.8 (Pologruto et al., 2003), using a 40×, 0.8 NA objective (Olympus) with a motorized stage and focus controls. We imaged green and red fluorescence simultaneously with two photomultiplier tubes behind red and green emission filters (FF01-593/40, FF03-525/50, Semrock) using a dichroic splitter (Di02-R561, Semrock) at a frame rate of 5 Hz over an area of 145 × 145 μm and at a resolution of 256 × 256 pixels. We imaged neurons in L2/3 at a depth of ~200 μm from pia. After identifying A1 L2/3 neurons responding to sounds, we presented different levels and frequencies of sounds (30, 50, and 70 dB SPL; 6, 12, 24, 32, 48, and 64 kHz; 500 ms duration, 20 ms ramps) while monitoring the changes in GCaMP6f fluorescence. We recorded neuronal activity in 10-s-long movies and presented sound stimuli 4 s after the start of each movie. We presented different sound stimuli every 30 s; each sound stimulus was presented three to five times. After obtaining movies of the responses to different sound stimuli, we began to infuse ZX1 solution into the cortex at a rate of 30 nl/min. Once ZX1 diffused in A1 (Fig. 1*c*, right), we reduced the pump speed to 9 nl/min and remeasured the responses of the same neurons to the same sounds. Mice were killed at the end of the recording session.

Two-photon imaging analysis. To quantify the neuronal responses to sounds, we identified neurons that were present in the field of view before and after ZX1 infusion and targeted only these cells for analysis. Using FluoroSNNAP software (Patel et al., 2015), we selected ROIs within the soma of each L2/3 neuron from the temporal average of each movie (50 frames, 10 s long). The pixels in each ROI from each frame were averaged and converted into $\Delta F/F$, as above. We then averaged the fluorescent response for three to five presentations of the same sound intensity and frequency for each neuron. Sound-evoked responses were measured for 1 s after the sound onset and were defined as responses if the sound-evoked changes in $\Delta F/F$ were larger than the mean plus 3 SDs of the baseline fluorescence measured before the sound onset. Responses were quantified as the integral of the increased fluorescence during this 1 s period. Best frequency (BF) was defined as the sound frequency resulting in the largest response independent of sound intensity (Kato et al., 2017). Receptive field bandwidth was defined as $\log_2$ of the ratio of the highest sound frequency and the lowest sound frequency that elicited a response from the neuron. For the analyses in Figures 1, *k* and *l*; 2, *h* and *i*; and 3*h–j*, for each neuron in control, response amplitudes were normalized to the minimum and maximum sound-evoked response amplitudes so that the normalized response amplitudes ranged from a minimum of 0 to a maximum of 1 (Barnstedt et al., 2015). For each neuron in ZX1, response amplitudes in ZX1 were normalized to the minimum and maximum sound-evoked response amplitudes of that neuron in control. A subset of neuronal sound-evoked responses to 12 kHz tones was also used in a previous study (Anderson et al., 2017). Namely, in Figure 1*f–l*, we used neuronal sound-evoked responses to 6, 12, 24, 32, 48, and 64 kHz tones from 232 neurons from nine mice. This dataset includes the sound-evoked responses to 12 kHz tones from 86 neurons from five mice, which were also included in the study by Anderson et al. (2017). In Figure 2*c–i*, we used neuronal sound-evoked responses to 6, 12, 24, 32, 48, and 64 kHz tones from 67 neurons from nine mice. This dataset includes the sound-evoked responses to 12 kHz tones from 40 neurons from six mice, which were also included in the study by Anderson et al. (2017). In Figure 3*c–j*, we used neuronal sound-evoked responses to 6, 12, 24, 32, 48, and 64 kHz tones from 81 neurons in 16 mice. This dataset includes the sound-evoked responses to 12 kHz tones from 12 neurons from four mice, which were also included in the study by Anderson et al. (2017).

Behavior. Frequency discrimination acuity was assessed by prepulse inhibition of acoustic startle responses (ASRs; Clause et al., 2011; Aizenberg and Geffen, 2013). Mice were placed in a sound-attenuation chamber (Coulbourn) on a load cell platform (Harvard Apparatus) that converted their movements into voltage waveforms. Animals were positioned in front of a calibrated speaker that delivered a continuous 70 dB SPL, 16 kHz tone (F1) with brief startle stimuli interspersed at random intervals (100 dB SPL broadband sounds, 6–26 kHz bandwidth, 40 ms in duration). The 100 dB SPL stimulus caused a reliable ASR. We quantified ASR amplitude as the maximum peak-to-peak amplitude of the voltage waveform from the platform for 500 ms after the onset of the startle stimulus minus the root mean square of the voltage waveform for 500 ms before the startle stimulus. For half of the startle trials, we changed the frequency of the continuous background tone to a different frequency (F2) for 80 ms before the onset of the startle stimulus. During each test session, we presented six different F2 stimuli in a random order five times each (15.4, 15.2, 14.4, 13.3, 12, and 10 kHz) and an equal number of randomly interleaved startle-only trials (16 kHz F2). Trials were randomly separated by an intertrial interval ranging from 8 to 24 s. We averaged the ASR amplitudes for each F2 and normalized these values to the ASR amplitude of startle-only trials. ASR inhibition is 1 minus the normalized ASR amplitude. To quantify the frequency discrimination threshold, we plotted the ASR inhibition versus the percent sound frequency change (F2 compared with F1). By fitting a sigmoid (logistic equation) line to this function, we quantified the frequency discrimination threshold ΔF_{50}, which is the percent change in sound frequency that caused 50% of the maximal ASR inhibition.

For prepulse inhibition experiments, we presented four different prepulse stimuli in a random order five times each (16, 15.4, 15.2, and 14.4 kHz; 50 ms duration, prepulse trials) and an equal number of randomly interleaved startle-only trials. Trials were randomly separated by an intertrial interval ranging from 8 to 24 s. Prepulse stimuli were completed 80 ms before the onset of the startle stimulus. We averaged the ASR amplitude for each prepulse stimulus frequency and normalized these values to the ASR amplitude of startle-only trials. Prepulse inhibition is 1 minus the normalized ASR amplitude for each prepulse stimulus.

Chronic cannula implants. To determine whether acute and localized disruptions of zinc signaling in auditory cortex impair two-tone sound frequency discrimination, we implanted bilateral chronic cannulas above the auditory cortex and infused either vehicle (saline) or ZX1 before behavioral testing. Following the same surgical approach as we did for viral injections, we implanted bilateral guide cannulas (22 gauge tubes, 13 mm length) into the skull medial to the stereotaxic location of A1 AAV injections (~3.5 mm lateral from lambda). Cannulas were affixed to the skull with dental acrylic and cyanoacrylate adhesive. Three to five days after implantation, we injected 1 μl of pH-buffered saline (vehicle) or saline containing 2 mM ZX1 into the cortex, via internal cannulas that were 0.5 mm longer than the guide cannulas (30 gauge, 13.5 mm length, Plastics One). Next, we assessed frequency discrimination or prepulse inhibition as described above. Based on the stereotaxic location of the cannulas, the lateral diffusion of Alexa Fluor 594 (Anderson et al., 2017), and relative locations of cortical areas in the mouse brain atlas (Paxinos et al., 2001), ZX1 was likely present throughout the auditory cortex, as well as visual and somatosensory cortices, during our behavioral testing. We allowed the mice to recover for at least 2 d and then infused either vehicle or ZX1 again. Each animal received an infusion of vehicle and an infusion of ZX1 on different days.

Auditory brainstem responses. Auditory brainstem response (ABR) thresholds were measured with subdermal electrodes in mice under isoflurane anesthesia (S. Li et al., 2013). We recorded auditory-evoked brainstem potentials after presenting broadband clicks (1 ms duration) and tones of 12, 16, and 32 kHz (3 ms duration), with a calibrated speaker (at a rate of 18.56 per second), via a probe tube inserted in the ear canal. We presented each sound 1024 times and analyzed the average evoked potential after bandpass filtering the waveform between 300 and 3000 Hz. The lowest sound intensity that generated ABR wave I amplitudes that were 4 SDs above the baseline noise level was classified as the ABR threshold. Baseline noise levels were measured using the ABRs obtained at 0 dB SPL sound intensity.

Experiments with KO mice. Experiments with WT and ZnT3 KO were blinded.

Statistics. Analysis was performed with MATLAB (Mathworks) and QuickCalcs (GraphPad). Group data are presented as mean ± SEM. For comparisons between multiple groups, we assessed overall differences with a one-way ANOVA or a one-way repeated-measures ANOVA for paired data (for normally distributed data) or the Kruskal–Wallis test or the Friedman test for paired data (for non-normally distributed data),

followed by pairwise comparisons using the Holm–Bonferroni's correction method. Pairwise comparisons were performed with the Student's paired *t* test, *t* test, or one-sample *t* test (for normally distributed data) or the Wilcoxon signed-rank or rank-sum tests (for non-normally distributed data). The normality of the distribution of data was assessed with the Lilliefors test. All tests were two-tailed.

Detailed values and statistical tests for all figures: Figure 1: ***f***, Overall control compared to ZX1: Friedman's $\chi^2 = 9.0$, $p = 0.003$; 30 dB SPL: control: 0.48 ± 0.06 octaves, ZX1: 0.76 ± 0.08 octaves, $p = 0.007$; 50 dB SPL: control: 0.93 ± 0.8 octaves, ZX1: 1.06 ± 0.08 octaves, $p = 0.17$; 70 dB SPL: control: 0.92 ± 0.08 octaves, ZX1: 1.24 ± 0.09 octaves, $p = 0.003$, signed-rank tests, $n = 232$ neurons from 9 mice). ***g***, Friedman's $\chi^2 = 8.62$, $p = 0.003$, 30 dB SPL: control: 0.88 ± 0.07 sound frequencies, ZX1: 1.08 ± 0.8 sound frequencies, $p = 0.04$; 50 dB SPL: control: 1.68 ± 0.10 sound frequencies, ZX1: 1.67 ± 0.09 sound frequencies, $p = 0.86$; 70 dB SPL: control: 1.52 ± 0.11 sound frequencies, ZX1: 1.82 ± 0.10 sound frequencies, $p = 0.001$, signed-rank tests, $n = 232$ neurons from 9 mice). ***k*** ,One-way repeated measures ANOVA F = 5.94, $p = 2.1e^{-5}$; 30 dB SPL: control: 0.60 ± 0.04, ZX1: 0.57 ± 0.04, $p = 0.69$; 50 dB SPL: control: 0.80 ± 0.04, ZX1: 0.60 ± 0.05, $p = 0.001$; 70 dB SPL: control: 0.73 ± 0.04, ZX1: 0.58 ± 0.03, $p = 0.0001$, paired *t* tests, $n = 232$ neurons from 9 mice). ***l***, One-way repeated measures ANOVA $F = 12.9$, $p = 1.1e^{-8}$; 30 dB SPL: control: 0.39 ± 0.01, ZX1: 0.52 ± 0.02, $p = 0.0004$; 50 dB SPL: control: 0.49 ± 0.01, ZX1: 0.58 ± 0.02, $p = 0.002$; 70 dB SPL: control: 0.49 ± 0.01, ZX1: 0.59 ± 0.02, $p = 4.5e^{-5}$, paired *t* tests, $n = 232$ neurons from 9 mice). ***m***, Friedman's $\chi^2 = 0.27$, $p = 0.27$; 30 dB SPL: control: 0.49 ± 0.12 octaves, Vehicle: 0.33 ± 0.09 octaves, $p = 0.29$; 50 dB SPL: control: 0.75 ± 0.16 octaves, Vehicle: 0.66 ± 0.14 octaves, $p = 0.14$; 70 dB SPL: control: 0.96 ± 0.19 octaves, Vehicle: 1.24 ± 0.17 octaves, $p = 0.50$, rank-sum tests, $n = 65$ neurons from 4 mice). ***n***, Kruskal-Wallace $\chi^2 = 5.01$, $p = 0.03$; 30 dB SPL: WT: 0.53 ± 0.06 octaves, ZnT3 KO: 1.17 ± 0.20 octaves, $p = 0.002$; 50 dB SPL: WT: 0.82 ± 0.07 octaves, ZnT3 KO: 1.23 ± 0.17 octaves, $p = 0.04$; 70 dB SPL: control: 0.86 ± 0.07 octaves, ZnT3 KO: 1.27 ± 0.18 octaves, $p = 0.02$, rank-sum tests, WT: $n = 297$ neurons from 13 mice; ZnT3 KO: $n = 56$ neurons from 3 mice). ***o***, Friedman's $\chi^2 = 1.88$, $p = 0.39$; 30 dB SPL: control: 1.17 ± 0.20 octaves, ZX1: 1.21 ± 0.20 octaves, $p = 0.87$; 50 dB SPL: control: 1.23 ± 0.17 octaves, ZX1: 1.20 ± 0.18 octaves, $p = 0.89$; 70 dB SPL: control: 1.27 ± 0.18 octaves, ZX1: 1.06 ± 0.18 octaves, $p = 0.42$, signed-rank tests, $n = 56$ neurons from 3 mice). ***p***, Near BF: WT control (black, $n = 916$ sound-evoked responses): 41.7 ± 2.5% Δ*F*/*F*, WT ZX1 (red): 30.8 ± 1.5% Δ*F*/*F*, $p = 0.0003$, paired *t* test; WT control, ZnT3 KO control (blue, $n = 284$ sound-evoked responses): 28.0 ± 2.7% Δ*F*/*F*, $p = 0.0025$, *t* test; ZnT3 KO control, ZnT3 KO ZX1 (red): 24.7 ± 2.2% Δ*F*/*F*, $p = 0.368$, paired *t* test. Away from BF: WT control (black $n = 685$ sound-evoked responses): 24.2 ± 1.4% Δ*F*/*F*, WT ZX1 (red): 32.6 ± 1.7% Δ*F*/*F*, $p = 0.0001$, paired *t* test; WT control, ZnT3 KO control (blue, $n = 197$ sound-evoked responses): 27.2 ± 2.8% Δ*F*/*F*, $p = 0.118$, *t* test test; ZnT3 KO control, ZnT3 KO ZX1 (red): 31.73 ± 3.60% Δ*F*/*F*, $p = 0.325$, paired *t* test.

Figure 2: ***c***, Friedman's $\chi^2 = 0.11$, $p = 0.74$; 30 dB SPL: control: 0.84 ± 0.14 octaves, ZX1: 0.61 ± 0.11 octaves, $p = 0.21$; 50 dB SPL: control: 1.33 ± 0.16 octaves, ZX1: 1.23 ± 0.14 octaves, $p = 0.76$; 70 dB SPL: control: 1.22 ± 0.13 octaves, ZX1: 1.64 ± 0.14 octaves, $p = 0.0092$, signed-rank tests, $n = 67$ neurons from 8 mice). ***d***, Friedman's $\chi^2 = 0.09$, $p = 0.88$; 30 dB SPL: control: 0.84 ± 0.14 sound frequencies, ZX1: 1.39 ± 0.17 sound frequencies, $p = 0.15$; 50 dB SPL: control: 2.46 ± 0.26 sound frequencies, ZX1: 2.29 ± 0.22 sound frequencies, $p = 0.57$; 70 dB SPL: control: 2.54 ± 0.23 sound frequencies, ZX1: 3.01 ± 0.22 sound frequencies, $p = 0.004$, signed-rank tests, $n = 67$ neurons from 8 mice). ***h***, One-way repeated measures ANOVA $F = 13.9$, $p = 1.2e^{-6}$; 30 dB SPL: control: 0.37 ± 0.03, ZX1: 0.45 ± 0.05, $p = 0.39$; 50 dB SPL: control: 0.57 ± 0.03, ZX1: 0.75 ± 0.06, $p = 0.002$; 70 dB SPL: control: 0.65 ± 0.03, ZX1: 0.82 ± 0.05, $p = 0.0007$, paired *t* tests, $n = 67$ neurons from 8 mice). ***I***, One-way repeated measures ANOVA $F = 20.1$, $p = 3.1e^{-9}$; 30 dB SPL: control: 0.37 ± 0.04, ZX1: 0.39 ± 0.05, $p = 0.76$; 50 dB SPL: control: 0.43 ± 0.03, ZX1: 0.63 ± 0.07, $p = 0.007$; 70 dB SPL: control: 0.46 ± 0.04, ZX1: 0.66 ± 0.08, $p = 0.01$, paired *t* tests, $n = 67$ neurons from 8 mice).

Figure 3: ***c***, Friedman's $\chi^2 = 0.66$, $p = 0.41$; 30 dB SPL: control: 0.72 ± 0.12 octaves, ZX1: 0.78 ± 0.13 octaves, $p = 0.71$; 50 dB SPL: control: 1.11 ± 0.15 octaves, ZX1: 0.89 ± 0.12 octaves, $p = 0.23$; 70 dB SPL: control: 1.57 ± 0.13 octaves, ZX1: 0.96 ± 0.13 octaves, $p = 0.0002$, signed-rank tests, $n = 81$ neurons from 16 mice. ***d***, Friedman's $\chi^2 = 0.98$, $p = 0.32$; 30 dB SPL: control: 2.67 ± 0.28 sound frequencies, ZX1: 2.73 ± 0.28 sound frequencies, $p = 0.58$; 50 dB SPL: control: 2.85 ± 0.27 sound frequencies, ZX1: 2.88 ± 0.28 sound frequencies, $p = 0.91$; 70 dB SPL: control: 3.71 ± 0.23 sound frequencies, ZX1: 3.22 ± 0.26 sound frequencies, $p = 0.0008$, signed-rank tests, $n = 81$ neurons from 16 mice. ***h***, One-way repeated measures ANOVA $F = 7.89$, $p = 0.0004$; 30 dB SPL: control: 0.43 ± 0.04, ZX1: 0.56 ± 0.05, $p = 0.02$; 50 dB SPL: control: 0.47 ± 0.04, ZX1: 0.56 ± 0.05, $p = 0.006$; 70 dB SPL: control: 0.57 ± 0.04, ZX1: 0.51 ± 0.05, $p = 0.21$, paired *t* tests, $n = 81$ neurons from 16 mice. ***I***, One-way repeated measures ANOVA $F = 5.76$, $p = 0.003$; 30 dB SPL: control: 0.49 ± 0.04, ZX1: 0.51 ± 0.05, $p = 0.70$; 50 dB SPL: control: 0.56 ± 0.04, ZX1: 0.50 ± 0.05, $p = 0.19$; 70 dB SPL: control: 0.64 ± 0.03, ZX1: 0.53 ± 0.04, $p = 0.014$, paired *t* tests, $n = 81$ neurons from 16 mice. ***j***, One-way repeated measures ANOVA $F = 3.59$, $p = 0.058$; 30 dB SPL: control: 0.56 ± 0.05, ZX1: 0.47 ± 0.06, $p = 0.17$; 50 dB SPL: control: 0.68 ± 0.05, ZX1: 0.61 ± 0.06, $p = 0.28$; 70 dB SPL: control: 0.82 ± 0.05, ZX1: 0.70 ± 0.07, $p = 0.047$, paired *t* tests, $n = 81$ neurons from 16 mice.

Figure 4: ***c***, One-way ANOVA, $F = 10.6$, $p = 2.55e^{-9}$. Compared with ASR at 16 kHz F2: 15.4 kHz, 79.1 ± 10.2%, $p = 0.07$; 15.2 kHz, 57.2 ± 7.2%, $p = 0.006$;14.4 kHz, 63.2 ± 7.6%, $p = 0.002$; 13.3 kHz, 46.8 ± 5.8%, $p = 0.0004$; 12 kHz, 34.3 ± 6.5%, $p = 0.0001$; 10 kHz, 36.3 ± 7.4%, $p = 1.97e^{-6}$; $n = 8$ mice, one-sample *t* tests. ***d***, One-way ANOVA, $F = 15.4$, $p = 1.64e^{-13}$. Compared with ASR at 16 kHz F2: 15.4 kHz, 119.8 ± 10.5%, $p = 0.09$; 15.2 kHz, 79.4 ± 9.6%, $p = 0.06$; 14.4 kHz, 94.9 ± 6.1%, $p = 0.69$; 13.3 kHz, 47.0 ± 9.6%, $p = 0.003$; 12 kHz, 43.3 ± 9.7%, $p = 0.0001$; 10 kHz, 39.1 ± 5.7%, $p = 5.75e^{-5}$; $n = 10$ mice, one-sample *t* tests. ***e***, WT: 3.7 ± 0.4% ΔF_{50}, $n = 8$ mice; KO: 12.7 ± 3.14% ΔF_{50}; $n = 10$ mice, $p = 0.022$, *t* test. ***h***, One-way ANOVA, $F = 0.63$, $p = 0.98$. Prepulse inhibition: 16 kHz prepulse: WT, 67.0 ± 9.1% versus KO, 61.7 ± 6.9%, $p = 0.64$; 15.4 kHz prepulse: WT, 60.1 ± 9.0% versus KO, 56.6 ± 5.3%, $p = 0.68$; 15.2 kHz prepulse: WT, 61.3 ± 5.4% versus KO, 57.1 ± 6.5%, $p = 0.64$; 14.4 prepulse: WT, 60.1 ± 5.5% versus KO, 62.0 ± 7.1%, $p = 0.90$; WT, $n = 8$ mice; KO, $n = 10$ mice; *t* tests. ***i***, Kruskal–Wallis $\chi^2 = 0.78$, $p = 0.38$. ABR wave I thresholds: WT ($n = 10$ mice) versus KO ($n = 8$ mice): click, 23.4 ± 3.0 dB SPL versus 29.5 ± 3.8 dB SPL, $p = 0.26$; 12 kHz, 23.8 ± 2.6 dB SPL versus 30.0 ± 2.6, $p = 0.17$; 16 kHz, 26.9 ± 3.5 dB SPL versus 27.0 ± 1.7 dB SPL, $p = 0.51$; 32 kHz, 26.8 ± 2.4 dB SPL versus 26.5 ± 1.8 dB SPL, $p = 0.98$, rank sum tests.

Figure 5: ***c***, One-way repeated-measures ANOVA, $F = 1.2$, $p = 0.34$. Compared with 16 kHz F2: 15.2 kHz F2: vehicle, 48.6 ± 9.2%, $p = 0.005$; ZX1, 75.6 ± 16.3%, $p = 0.21$; 14.4 kHz: vehicle, 43.5 ± 2.8%, $p = 9.6e\text{-}6$; ZX1, 38.7 ± 7.5%, $p = 0.001$; $n = 5$ mice one-sample *t* tests. ***e***, One-way repeated-measures ANOVA, $F = 1.38$, $p = 0.27$. Prepulse inhibition: 16 kHz prepulse; control, 77.4 ± 6.7% versus ZX1, 76.3 ± 8.7%, $p = 0.92$; 15.2 kHz prepulse; control, 80.9 ± 3.3% versus ZX1, 78.4 ± 5.1%, $p = 0.69$; 14.4 kHz prepulse; control, 74.1 ± 1.5% versus ZX1, 76.6 ± 4.8, *p* 0.64, $n = 5$ mice, *t* tests. ***f***, One-way repeated-measures ANOVA, $F = 3.3$, $p = 0.048$. Compared with ASR at 16 kHz F2: 15.2 kHz: control, 114.3 ± 18.9%, $p = 0.70$; ZX1, 77.3 ± 8.0%, $p = 0.06$; 14.4 kHz: control, 77.1 ± 10.6%, $p = 0.19$; ZX1, 83.6 ± 11.4%, $p = 0.24$; 13.3 kHz: control, 62.3 ± 3.0%, $p = 0.001$; ZX1, 67.1 ± 4.6%, $p = 0.005$, $n = 4$ mice, one-sample *t* tests.

Results

We began our investigation by localizing the primary auditory cortex (A1). To do this, we visualized cortical neuronal sound-evoked responses by using *in vivo* wide-field transcranial fluorescent imaging in head-fixed unanesthetized (awake) mice (Fig. 1*a*). To visualize neuronal sound-evoked responses, we used AAV driven by the calcium/calmodulin-dependent protein kinase 2 promoter to express the genetically encoded calcium indicator GCaMP6f in principal neurons in the auditory cortex (Chen et al., 2013; Pakan et al., 2016; AAV-CaMKII-GCaMP6f; see Materials and Methods). We presented low-frequency tones (6 kHz, 50–60 dB SPL) and imaged the sound-evoked changes in

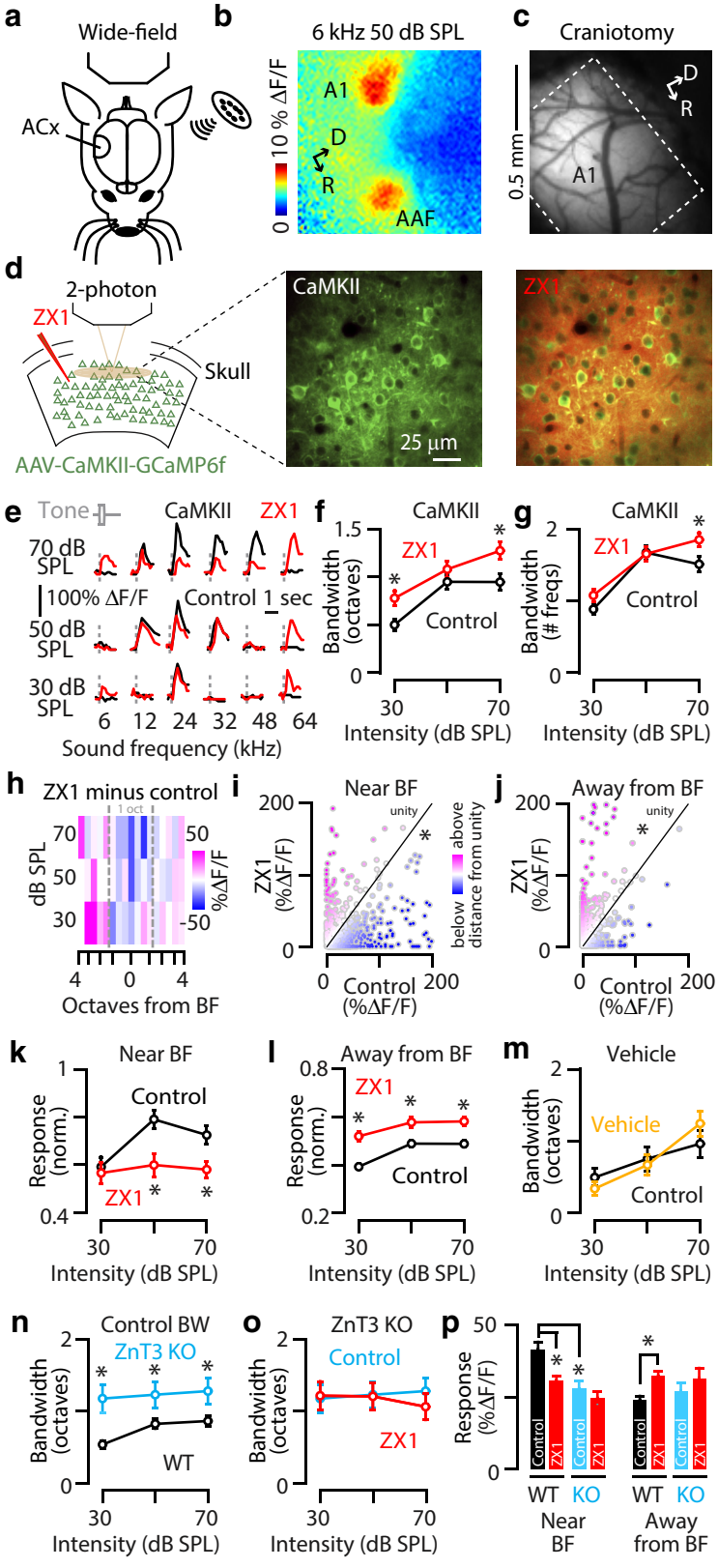

Figure 1. Synaptic zinc sharpens the frequency tuning of A1 L2/3 principal neurons. ***a***, Schematic of an experimental setup illustrating transcranial imaging using GCaMP6f in a head-fixed awake mouse. Sounds are delivered through a calibrated speaker. ACx, auditory cortex. ***b***, A 6 kHz, 50 dB SPL tone triggered GCaMP6f fluorescence responses in two discrete regions of the auditory cortex representing primary auditory cortex (A1) and the AAF. D, Dorsal; R, rostral. ***c***, Image illustrating a craniotomy over primary auditory cortex (A1). D, Dorsal; R, rostral. ***d***, Left, Schematic of an experimental setup illustrating two-photon imaging of GCaMP6f in principal neurons. Middle, Image of a population of A1 L2/3 principal neurons. Right, The same neurons as in the middle after ZX1 infusion. ***e***, Representative example of the receptive fields of an A1 L2/3 principal neuron in control (black) and after ZX1 (red). ***f***, Average effect of ZX1 (red) on the receptive field bandwidth of L2/3 principal neurons at different sound intensities [control (black) vs ZX1: 30 dB SPL, $p = 0.007$; 70 dB SPL, $p = 0.003$; $n = 232$ neurons from 9 mice, signed-rank tests]. ***g***, Average effect of ZX1 (red) on the number of sound frequencies a neuron responds to [control (black) vs ZX1: 70 dB SPL, $p = 0.001$; signed-rank test]. ***h***, Heat map showing the average change in response amplitudes after ZX1 infusion (amplitude in ZX1 minus amplitude in control) to tone frequencies below, near, and above BF: pink indicates larger response amplitudes after ZX1, and blue indicates smaller response amplitudes after ZX1. ***i***, Scatter plots of sound-evoked responses in control versus ZX1 for all sound intensities and frequencies near BF (compared with unity, $p = 4.4e^{-5}$, one-sample *t* test). ***j***, Same as ***i*** but to tone frequencies away from BF compared with unity ($p = 0.026$, one-sample *t* test). We observed that 16.3% of neurons developed a response to a sound frequency that had not evoked a response in control, whereas 12.9% of neurons lost a response to a sound frequency that had evoked a response in control. ***k***, Average effect of ZX1 (red) on the sound-evoked response amplitudes of principal neurons to tones with frequencies within 1 octave from the BF [control (black) vs ZX1: 50 dB SPL, $p = 0.001$; 70 dB SPL, $p = 0.0001$]. ***l***, Average effect of ZX1 (red) on the sound-evoked response amplitudes of principal neurons to tones with frequencies >1 octave away from BF [control (black) vs ZX1: 30 dB SPL, $p = 0.0004$; 50 dB SPL, $p = 0.002$; 70 dB SPL, $p = 4.5e\text{-}5$]. ***m***, Same as in ***f*** but in but after vehicle infusion. ***n***, Average receptive field bandwidths (BW) in control for WT and ZnT3 KO [WT (black) vs ZnT3 KO (blue): 30 dB SPL, $p = 0.0023$; 50 dB SPL, $p = 0.0392$; 70 dB SPL, $p = 0.0188$; $n = 290$ neurons from 13 mice in WT, $n = 56$ neurons from 3 mice in ZnT3 KO, rank sum tests.) ***o***, Same as in ***f*** but in ZnT3 KO. ***p***, Average sound-evoked response amplitudes to sounds with frequencies near BF (left) and away from BF (right) for WT and ZnT3 KO mice. Near BF: WT control (black) versus WT ZX1 (red), $p = 0.0003$; WT control vs ZnT3 control (blue), $p = 0.0025$. Away from BF: WT control vs WT ZX1, $p = 0.0001$. For all panels, asterisks indicate significant differences after accounting for multiple comparisons using the Holm–Bonferroni's correction; error bars indicate SEM. Detailed values and statistical tests are listed in the Materials and Methods.

GCaMP6f fluorescence (Fig. 1*b*; see Materials and Methods). Because of the mirror-like reversal of tonotopic gradients between A1 and the AAF (Guo et al., 2014; Joshi et al., 2015), these sounds activated two discrete regions of the auditory cortex corresponding to the low-frequency regions of A1 and the AAF (Fig. 1*b*). These results are consistent with previous mapping of mouse A1 (Guo et al., 2014; Issa et al., 2014; Joshi et al., 2015).

After A1 localization, to examine the effects of zinc signaling on the frequency tuning of individual A1 L2/3 principal neurons, we anesthetized the animal to perform a small craniotomy over A1 and removed the anesthesia to undertake two-photon imaging in awake mice (Fig. 1*c*,*d*; see Materials and Methods). We identified sound-responsive neurons and presented sounds of different frequencies and intensities to measure the tonal receptive

fields of L2/3 neurons in A1 (Fig. 1*e*, black traces). To test the effect of endogenous, extracellular zinc on frequency tuning, we infused the extracellular, high-affinity, fast, zinc-specific chelator ZX1 (Pan et al., 2011; Anderson et al., 2015), through a thin-glass micropipette (Fig. 1*d*, left; see Materials and Methods). To verify the intracortical diffusion of the chelator into A1, we visualized the spread of the extracellular red fluorescent dye Alexa Fluor 594, which was coinfused with ZX1 (Fig. 1*d*, right). This approach leads to $\sim$2 mm^2 of cortical surface area with detectable red fluorescence (Anderson et al., 2017), confirming the spread of ZX1 throughout the auditory cortex. After ZX1 diffusion, we were able to locate the same neurons (Fig. 1*d*, middle and right) to remeasure their sound-evoked activity (Fig. 1*e*, red traces). ZX1 widened the range of sound frequencies, termed bandwidth, in A1 L2/3 principal neurons' receptive fields, to tones of 30 and 70 dB SPL intensity. Moreover, ZX1 increased the number of sound frequencies in the receptive field at 70 dB SPL (Fig. 1*e–g*). These results suggest that zinc sharpens the frequency tuning of principal neurons. Because zinc enhances the gain of principal neurons in response to 12 kHz tones (Anderson et al., 2017), we hypothesized that the enhancing effects of zinc on gain and the sharpening effects of zinc on frequency tuning occur at different sound frequency regions within the neuronal receptive field. To explore this, we created a heat map showing the average pairwise differences of sound-evoked response amplitudes in ZX1 minus the control response for different sound frequencies compared with BF (Fig. 1*h*). We observed a general reduction in response amplitudes near BF, indicated by the prevalence of the blue color, and a general increase in response amplitudes away from BF, indicated by the prevalence of the pink color. For further analysis, we divided the sound-evoked responses into two groups: near BF responses occurring within an octave of BF and away-from BF responses occurring more than one octave away from BF. To explore the effects of extracellular zinc on these different sound frequency regions, we plotted the sound-evoked response amplitude for each sound frequency and intensity in control versus the response amplitude evoked by the same sound frequency and intensity in ZX1. This analysis revealed that the change in sound-evoked response amplitudes to sounds with frequencies near BF were, on average, significantly below unity, indicating that ZX1 caused a reduction in response amplitudes at these sound frequencies (Fig. 1*i*). In contrast, the change in response amplitudes to sounds with frequencies away from BF was, on average, significantly above unity, indicating that ZX1 caused an increase in response amplitudes at these sound frequencies (Fig. 1*j*). To further quantify these changes, we analyzed response amplitudes for each group as a function of sound intensity. For sounds with frequencies near BF, ZX1 caused a significant reduction in response amplitudes to tones of 50 and 70 dB SPL intensity (Fig. 1*k*). However, for sounds with frequencies away from BF, ZX1 enhanced the response amplitudes to tones of 30, 50, and 70 dB SPL intensity (Fig. 1*l*). The effects of ZX1 were not attributable to nonspecific issues related to the injection of fluid into auditory cortex, because vehicle injections containing ACSF and Alexa Fluor 594 did not affect the bandwidth of A1 principal neurons (Fig. 1*m*). Together, these results indicate that endogenous extracellular zinc has dual effects on principal neurons: (1) consistent with previous observations (Anderson et al., 2017), zinc increases the response gain of A1 principal neurons by enhancing responses to sounds with frequencies near BF; and (2) zinc sharpens the frequency tuning of A1 principal neurons by suppressing responses to sounds with frequencies away from BF.

To track the origin of the extracellular zinc that sharpened frequency tuning, we performed similar experiments in ZnT3 KO mice, which lack the vesicular zinc transporter ZnT3 and thus synaptic zinc (Cole et al., 1999). The bandwidth of L2/3 principal neurons in ZnT3 KO mice was significantly wider than in WT mice (Fig. 1*n*). Moreover, zinc chelation with ZX1 did not affect the bandwidth of principal neurons in ZnT3 KO mice (Fig. 1*o*). Together, these results indicate that ZnT3-dependent, extracellular synaptic zinc signaling sharpens the frequency tuning of A1 L2/3 principal neurons.

To further explore whether acute disruptions of synaptic zinc in WT mice by ZX1 infusion had effects similar to genetic elimination of synaptic zinc in ZnT3 KO mice, we compared the effects of these two manipulations on sound-evoked responses. We found that both ZX1 and ZnT3 deletion led to a similar reduction in response amplitudes to sounds with frequencies near BF (Fig. 1*p*, left). However, ZX1 enhanced the response to sounds with frequencies away from BF, whereas ZnT3 deletion did not [WT control is not different from ZnT3 KO control in Fig. 1*p* (right)], suggesting that developmental changes or adaptation mechanisms in ZnT3 KO mice might contribute to this difference. Because the ZX1-mediated suppression (near BF) and enhancement (away from BF) of responses does not occur in ZnT3 KO mice (Fig. 1*p*), these results also suggest that tonic zinc, which is independent of ZnT3 (Anderson et al., 2015), is not a major contributor to the zinc-mediated effects of zinc on principal neuron responses.

To investigate the cellular mechanisms underlying the effect of synaptic zinc on the frequency tuning of L2/3 principal neurons, we next explored the effect of zinc on the frequency tuning of L2/3 PV-expressing interneurons (PV neurons), which inhibit principal neurons (Harris and Shepherd, 2015; Tremblay et al., 2016). To achieve this, we selectively expressed GCaMP6f in PV neurons by injecting AAV-Flex-GCaMP6f into the auditory cortex of PV-Cre mice (Fig. 2*a*; see Materials and Methods). ZX1 increased the bandwidth of A1 L2/3 PV neurons to tones of 70 dB SPL intensity (Fig. 2*b*,*c*) and increased number of sound frequencies that drove significant sound-evoked responses at 70 dB SPL (Fig. 2*d*). These results suggest that zinc sharpens the frequency tuning of PV neurons. In contrast to the dual effects of ZX1 on principal neurons, in PV neurons, ZX1 enhanced responses to all tested sound frequencies and to most tested sound intensities (Fig. 2*e–i*). This is consistent with our previous report of zinc reducing the gain of PV neurons in response to 12 kHz tones (Anderson et al., 2017) and shows that the suppressive effects of zinc on PV neuron response amplitudes occur over a broad range of sound frequencies and intensities. Although our approach involving the bulk application of ZX1 is not conclusive for distinguishing cell-dependent (direct) versus network-dependent effects, the zinc-mediated decreases in response amplitudes of PV neurons to sounds with frequencies near BF (Fig. 2*h*) are consistent with the zinc-mediated increases in response amplitudes of principal neurons to sounds with frequencies near BF (Fig. 1*k*) and suggest a linear, potentially direct link between the zinc modulation of A1 L2/3 PV and principal neuron responses to sounds with frequencies near BF. However, the inhibitory effects of zinc on A1 L2/3 PV neuron responses to sounds with frequencies away from BF (Fig. 2*i*) are not contributing, at least not directly, to the zinc-mediated inhibition of A1 L2/3 principal neuron responses to sounds with frequencies away from BF (Fig. 1*l*). This result also suggests that zinc-mediated modulation of a different type of interneuron might be contributing to the sharpening of frequency tuning of principal neurons.

Next, we therefore tested the effect of zinc on the tuning of SOM-expressing interneurons (SOM neurons), which inhibit principal neurons and PV neurons (Harris and Shepherd, 2015; Tremblay et al., 2016). To do this, we selectively expressed GCaMP6f in SOM neurons by injecting AAV-Flex-GCaMP6f into the auditory cortex of SOM-Cre mice (Fig. 3*a*). Application of ZX1 decreased the bandwidth of A1 L2/3 SOM neurons to tones of 70 dB SPL intensity (Fig. 3*b*,*c*) and decreased the number of sound frequencies that drove significant sound-evoked response at 70 dB SPL (Fig. 3d). Because zinc reduced the gain of SOM neurons in response to 12 kHz tones (Anderson et al., 2017), we hypothesized that the suppressive effects of zinc on gain and the broadening effects of zinc on frequency tuning occur at different sound frequency regions within the neuronal receptive field. On average, ZX1 enhanced responses to sounds with frequencies below BF (Fig. 3*e*,*f*,*h*), suppressed responses to sounds with frequencies above BF (Fig. 3*e*,*g*,*i*), and did not affect sound-evoked responses to sounds with frequencies at BF (Fig. 3*e*,*j*). The zinc-mediated enhancement of A1 L2/3 SOM responses to sounds with frequencies above BF (Fig. 3*i*) is consistent with the zinc-mediated reduction in response amplitudes of A1 L2/3 principal and PV neurons to sounds with frequencies away from BF and suggest a linear, potentially direct, relationship between the zinc-mediated modulation of SOM neurons and principal and PV neurons. However, the zinc-mediated reduction in A1 L2/3 SOM responses to sounds with frequencies below BF (Fig. 3*h*) is not consistent with the zinc-mediated reduction in response amplitudes of A1 L2/3 principal and PV neurons to sounds with frequencies away from BF. These results suggest that the effects of zinc on sound frequencies below BF potentially arise from network-level effects of zinc on A1 (see Discussion). Together, our results show that the effect of synaptic zinc on frequency tuning is cell specific. Synaptic zinc sharpens the frequency tuning of A1 L2/3 PV neurons and principal neurons and widens the frequency tuning of A1 L2/3 SOM neurons.

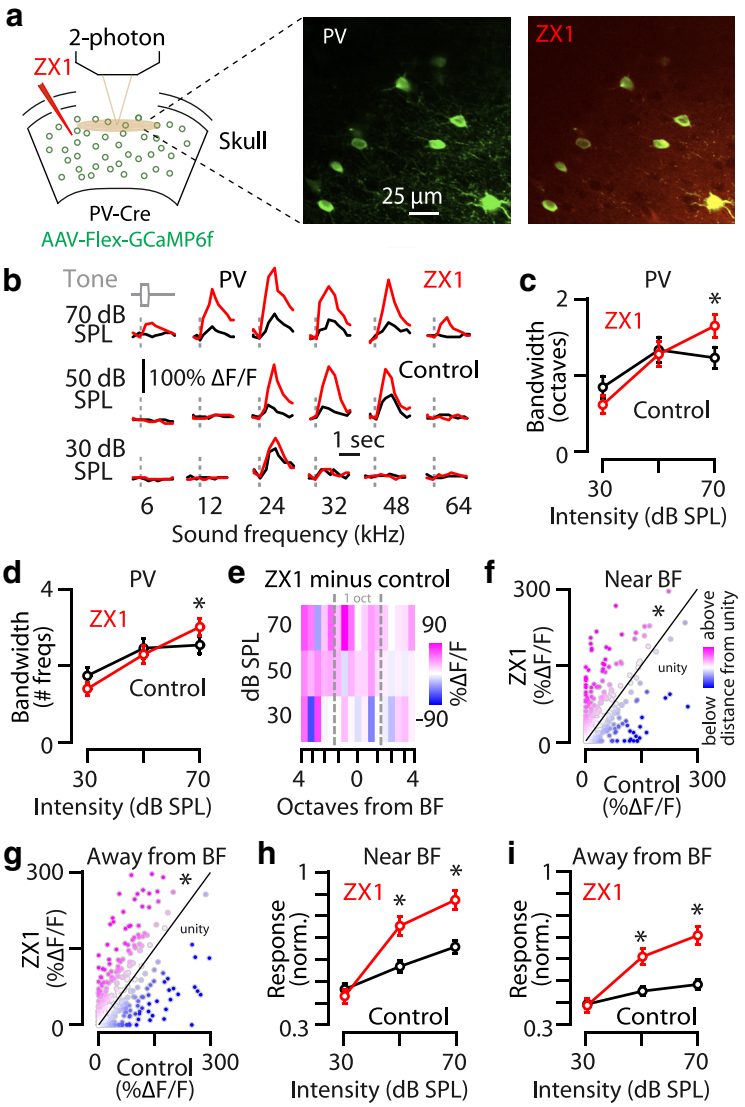

Figure 2. Synaptic zinc sharpens the frequency tuning of A1 L2/3 PV neurons. ***a***, Left, Schematic of the experimental setup illustrating two-photon imaging of GCaMP6f in PV neurons. Middle, Image of a population of A1 L2/3 PV neurons. Right, The same neurons as in the middle after ZX1 infusion. ***b***, Representative example of the receptive fields of an A1 L2/3 PV neuron in control (black) and after ZX1 infusion (red). ***c***, Average effect of ZX1 (red) on the receptive field bandwidth of L2/3 PV neurons at different sound intensities [ZX1 vs control (black); 70 dB: $p = 0.0092$, signed-rank test, $n = 67$ neurons from 8 mice]. ***d***, Average effect of ZX1 (red) on the number of sound frequencies a neuron responds to [control (black) vs ZX1; 70 dB SPL, $p = 0.004$]. ***e***, Heat map showing the average change in response amplitudes after ZX1 infusion (amplitude in ZX1 minus amplitude in control) to tone frequencies below, near, and above BF: pink indicates larger response amplitudes after ZX1, and blue indicates smaller response amplitudes after ZX1. ***f***, Scatter plots of sound-evoked responses at all intensities to tone frequencies near BF for control versus ZX1; compared with unity, $p = 0.02$, one-sample *t* test. ***g***, Same as ***f*** but to sound frequencies away from BF; compared with unity, $p = 0.008$, one-sample *t* test. We observed that 16.4% of neurons developed a response to a sound frequency that had not evoked a response in control, whereas 10.9% of neurons lost a response to a sound frequency that had evoked a response in control. ***h***, Average effect of ZX1 (red) on the sound-evoked response amplitudes of A1 L2/3 PV neurons to tones with frequencies within 1 octave from BF [control (black) vs ZX1; 50 dB SPL, $p = 0.002$; 70 dB SPL, $p = 0.0007$]. ***i***, Average effect of ZX1 (red) on the sound-evoked response amplitudes of A1 L2/3 PV neurons to tones with frequencies >1 octave away from BF [control (black) vs ZX1; 50 dB SPL, $p = 0.007$; 70 dB SPL, $p = 0.012$]. For all panels, asterisks indicate significant differences after accounting for multiple comparisons using the Holm-Bonferroni's correction; error bars indicate SEM. Detailed values and staticistcal test are listed in the Materials and Methods.

To explore whether the cellular- and system-level effects of synaptic zinc on A1 neuron frequency tuning support acuity for sound frequency-driven behaviors, we examined whether disruptions in synaptic zinc signaling impair the ability of mice to discriminate sounds of different frequencies. To answer this question, we used a behavioral task based on prepulse inhibition of the acoustic startle response: mice startle in response to loud sounds, startle stimuli, and inhibit this startle response when the startle stimulus is preceded by a prepulse, which is a nonstartling stimulus. Before the onset of the startle stimulus, we presented prepulse tone stimuli with frequencies (F2) that were different from a continuous background tone stimulus of 16 kHz (F1; Fig. 4*a*). We then quantified the percent change between F1 and F2 that led to half-maximal

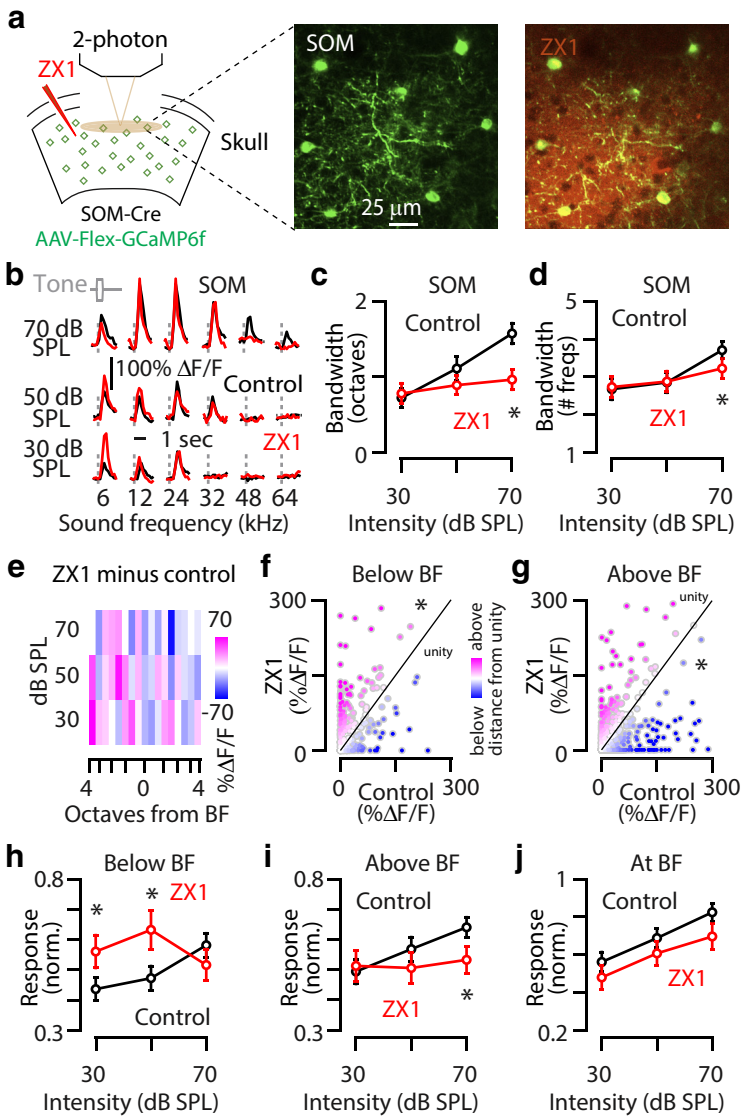

Figure 3. Synaptic zinc widens tuning of A1 L2/3 SOM neurons. ***a***, Schematic of the experimental setup illustrating two-photon imaging of GCaMP6f in SOM neurons. Middle, Image of a population of A1 L2/3 SOM neurons. Right, The same neurons as in the middle after ZX1 infusion. ***b***, Representative example of the receptive fields of an A1 L2/3 SOM neuron in control (black) and after ZX1 infusion (red). ***c***, Average effect of ZX1 (red) on the receptive field bandwidth of L2/3 SOM neurons at different sound intensities [ZX1 vs control (black): 70 dB: $p = 0.0002$, signed-rank test, $n = 81$ neurons from 16 mice]. ***d***, Average effect of ZX1 (red) on the number of sound frequencies a neuron responds to [control (black) vs ZX1;70 dB SPL, $p = 0.0008$]. ***e***, Heat map showing the average change in response amplitudes after ZX1 infusion (amplitude in ZX1 minus amplitude in control) to tone frequencies below, near, and above BF: pink indicates larger response amplitudes after ZX1, and blue indicates smaller response amplitudes after ZX1. ***f***, Scatter plot of sound-evoked responses at all intensities to tone frequencies below BF for control versus ZX1; compared with unity, $p = 0.003$, one-sample t test. ***g***, Same as ***f*** but to tone frequencies above from BF; compared with unity, $p = 0.03$, one-sample t test. We observed that 6.7% of neurons developed a response to a sound frequency that had not evoked a response in control, whereas 15.7% of neurons lost a response to a sound frequency that had evoked a response in control. ***h***, Average effect of ZX1 (red) on the sound-evoked response amplitudes of A1 L2/3 SOM neurons to tones with frequencies more below BF [control (black) vs ZX1; 30 dB SPL, $p = 0.02$; 50 dB SPL, $p = 0.006$]. ***i***, Average effect of ZX1 (red) on the sound-evoked response amplitudes of A1 L2/3 SOM neurons to tones with frequencies above from BF control (black) versus ZX1 (70 dB SPL, $p = 0.014$). ***j***, Average effect of ZX1 (red) on the sound-evoked response amplitudes of A1 L2/3 SOM neurons to tones with frequencies at BF control (black). For all panels, asterisks indicate significant differences after accounting for multiple comparisons using the Holm-Bonferroni's correction; error bars indicate SEM. Detailed values and staticistcal test are listed in the Materials and Methods.

inhibition of the startle response (Clause et al., 2011; Aizenberg and Geffen, 2013). Whereas WT mice detected ~4% differences between F1 and F2 tones as evidenced by inhibition of their acoustic startle responses (Fig. 4*b–e*), ZnT3 KO mice showed significantly impaired sound frequency discrimination and were unable to discriminate F2 tones until their frequencies were ~13% different from F1 (Fig. 4*b–e*). These results show that synaptic zinc plays a crucial role in improving the acuity of sound frequency discrimination.

Deficits in sound frequency discrimination in ZnT3 KO mice were not attributable to temporal processing deficits or other general behavioral problems, because prepulse inhibition was not different between WT and ZnT3 KO mice when individual tones were presented as prepulse stimuli against a quiet background (Fig. 4*f–h*). This result is consistent with previous studies comparing prepulse inhibition between WT and ZnT3 KO mice (Cole et al., 2001; Thackray et al., 2016). Moreover, deficits in sound frequency discrimination in ZnT3 KO mice were not caused by hearing loss, because WT and ZnT3 KO mice did not have different hearing thresholds (Fig. 4*i*). We assessed hearing thresholds by determining the minimal sound intensity causing a detectable synchronous activity of auditory nerve and auditory brainstem nuclei, termed auditory brainstem response. Together, these results show that synaptic zinc signaling improves the ability to discriminate two tones with different frequencies—a crucial aspect of auditory processing—without affecting hearing thresholds or detection of individual sound stimuli.

The behavioral deficits observed in ZnT3 KO mice were not attributable to either developmental abnormalities or nonspecific disruption of zinc signaling in auditory cortex, because transient, cortical ZX1 infusion, but not vehicle infusion, impaired frequency discrimination performance in WT mice without affecting their ability to detect single tones (Fig. 5*a–e*). The infusion of ZX1 in the cortex of WT mice disrupted the ability to discriminate between sounds with subtle frequency differences: changes from 16 kHz to 15.2 kHz were undetectable (Fig. 5*c*). However, ZnT3 deletion led to more severe deficits: changes from 16 kHz to 14.4 kHz were undetectable (Fig. 4*d*). The more robust effect of ZnT3 deletion is consistent with the involvement of multiple brain areas to this behavioral task, including the dorsal cochlear nucleus (Davis et al., 1982; Meloni and Davis, 1998), which contains high levels of synaptic zinc (Kalappa et al., 2015). Finally, ZX1 infusion into the cortex of ZnT3 KO mice did not affect sound frequency discrimination, supporting the conclusion that the effects of ZX1 are caused by its interference with cortical synaptic zinc signaling (Fig. 5*f*). Together, these results reveal cortical synaptic zinc as a novel modulator of frequency tuning and sound frequency discrimination.

Discussion

The role of synaptic zinc in modulating cortical frequency tuning

Our findings complement and expand previous studies showing that enhancement or suppression of cortical sensory representations have a direct impact on auditory processing acuity (Froemke et al., 2013; Aizenberg et al., 2015; Sohoglu and Chait, 2016; Guo et al., 2017). Synaptic zinc increases the gain of responses to sounds with frequencies near BF and simultaneously sharpens the receptive fields of A1 L2/3 principal neurons, by reducing responses to sounds with frequencies away from BF. This dual modulation improves sound frequency discrimination and increases responsiveness to preferred sounds concurrently. This is different from the auditory cortical mechanism involving a corticothalamic circuit allowing either increased feature detection at the expense of discrimination or sharper discrimination at the expense of feature detection (Guo et al., 2017). Although systemic nicotine increases both feature detection and discrimination in the auditory system, this dual modulation involves cortical and subcortical actions (Askew et al., 2017). Therefore, we propose that synaptic zinc provides a unique cortical signaling pathway capable of concurrently allowing enhanced feature detection and discrimination.

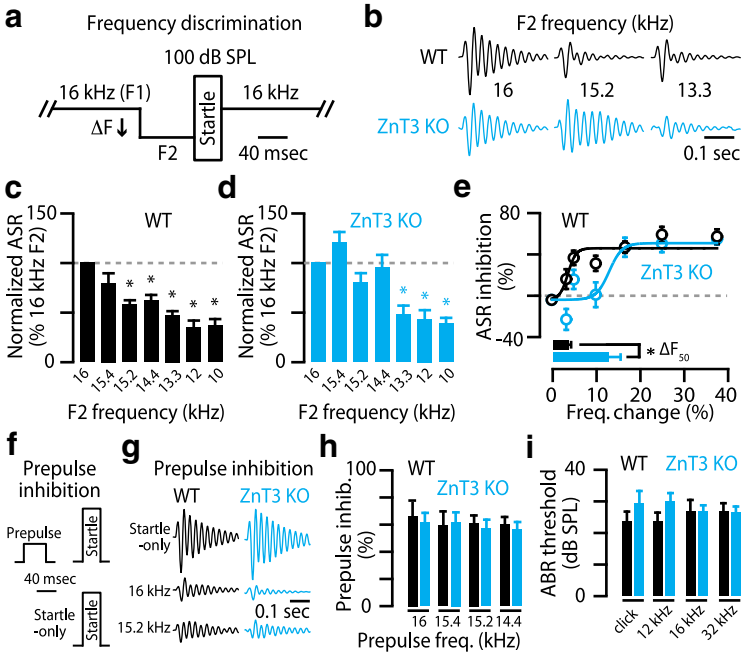

Figure 4. ZnT3 KO mice have poor frequency discrimination acuity. ***a***, Schematic illustrating the sound frequency discrimination acuity behavioral test. ***b***, Examples of acoustic startle response (ASR) waveforms of WT (black) and ZnT3 KO (blue) mice for different F2 frequencies. F1 is set at 16 kHz. ***c***, Summary graph showing ASR amplitudes as a function of F2 in WT mice (normalized to 16 kHz F2, $p \leq 0.006$, $n = 8$ mice, one-sample *t* tests). ***d***, Same as in ***c*** but in ZnT3 KO ($p \leq 0.003$, $n = 10$ mice, one-sample *t* tests). ***e***, Sigmoid fits (lines) and average values (circles) showing ASR inhibition as a function of percent changes between F2 and F1. In the inset, the average bar graph shows the frequency discrimination threshold (ΔF_{50}; for WT (black) and ZnT3 KO (blue), $p = 0.022$, *t* test, $n = 8$ WT and 10 ZnT3 KO mice). ***f***, Schematic illustrating the prepulse inhibition behavioral task. ***g***, Examples of ASR waveforms of WT (black) and KO mice (blue). ***h***, Summary graph showing prepulse inhibition for different prepulse stimuli in WT (black, $n = 8$ mice) and KO (blue, $n = 10$ mice). ***i***, Summary graph showing ABR thresholds of WT (black, $n = 8$) and ZnT3 KO (blue, $n = 10$). For all panels, asterisks indicate significant differences after accounting for multiple comparisons using the Holm-Bonferroni's correction; error bars indicate SEM. Detailed values and staticistcal test are listed in the Materials and Methods.

Currently, there are three major models to explain the tuning of auditory cortical neurons: (1) the "iceberg" model, in which excitation and inhibition are balanced or cotuned and frequency tuning is achieved because only the strongest excitatory input drives the cell to spike threshold (Wehr and Zador, 2003; Zhang et al., 2003; Moore and Wehr, 2013); (2) the approximately balanced model, in which inhibition is relatively stronger than excitation in frequency domains away from the preferred frequencies (Wu et al., 2008; Li et al., 2014); and (3) the lateral inhibition model, in which inhibition, through network mechanisms, inhibits wide regions of cortical space (Priebe and Ferster, 2008; Kato et al., 2017). The role of synaptic zinc signaling in shaping cortical frequency tuning has important implications for all these models. For the iceberg model, where the strength of excitation and inhibition are balanced, synaptic zinc contributes to a balance of excitation and inhibition leading to higher levels of activity in principal neurons to sounds with frequencies near BF. Because the sound-evoked responses of L2/3 PV neurons contribute strong inhibition around the BF of L2/3 principal neurons (Li et al., 2014), we suggest that the suppression of PV neuron responses by synaptic zinc allows for a wider range of sound frequencies and sound intensities around BF to drive spiking responses in L2/3 principal neurons. For the approximately balanced model, where inhibition is relatively stronger than excitation in frequency domains away from the preferred frequencies, synaptic zinc provides a mechanism allowing wider frequency tuning of SOM neurons because it enhances the responses of SOM neurons to sounds with frequencies above their BF. Finally, for the lateral inhibition model, previous studies in the auditory and visual system have attributed lateral inhibition to the activity of SOM neurons (Adesnik et al., 2012; Kato et al., 2017). In light of recent work highlighting the contribution of SOM neuron activity to network-mediated lateral inhibition that is asymmetrical with respect to BF (Kato et al., 2017), it is interesting that the enhancing and suppressing effects of zinc on the sound-evoked responses of SOM neurons are also asymmetric with respect to BF. Therefore, we propose that the enhancing effect of zinc signaling on SOM neuron responses to sounds with frequencies above BF might serve to enhance lateral inhibition for these sound frequencies in A1 (Kato et al., 2017). Since these three models are not mutually exclusive but rather describe different points along a continuum of cortical operating regimes (Levy and Reyes, 2011; McGinley et al., 2015), our study contributes additional mechanistic understanding to how inhibition is able to shape cortical frequency tuning.

Because in recent years the focus of cortical inhibition research has shifted from cellular or single synapse effects to network effects, it is important to consider the effects of synaptic zinc in the context of network effects. Currently, there are two network models capable of explaining network effects of inhibition in the auditory cortex: the inhibition stabilized network model (Kato et al., 2017), mostly based on the power of recurrent inhibition (Ozeki et al., 2009), and the cascaded feedforward model, mostly based on multiple stages of feedforward inhibition (Moore et al., 2018). Both models, which are not mutually exclusive, can explain paradoxical effects of how decreased inhibition

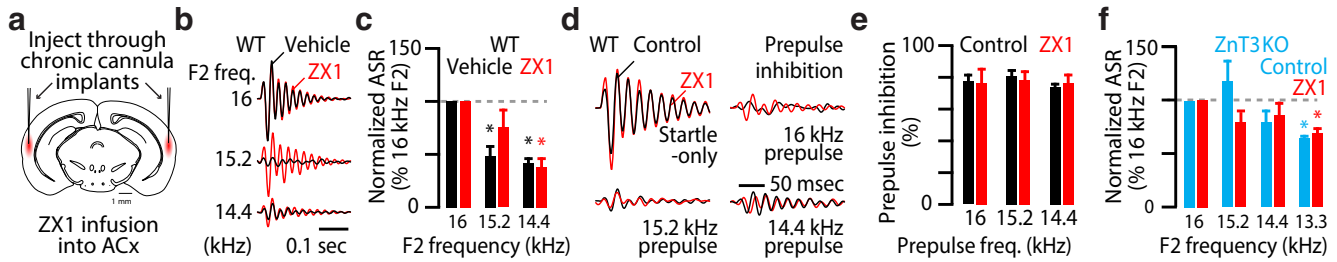

Figure 5. Cortical synaptic zinc signaling improves sound frequency discrimination. ***a***, Schematic illustrating the placement of bilateral chronic cannulas over the auditory cortex (ACx) for local ZX1 infusion. Cartoon of brain adapted from (Paxinos and Fraklin, 2001). ***b***, Examples of ASR waveforms after ZX1 (red) or vehicle (black) infusions. ***c***, Summary graph showing ASR amplitudes after ZX1 (red) or vehicle (black) infusion in WT (normalized to 16 kHz F2: for vehicle or ZX1 vs 16 kHz, $p \leq 0.005$, $n = 5$ mice, one-sample *t* tests). ***d***, Examples of ASR waveforms after different prepulse stimuli before (control, black) and after (red) ZX1. ***e***, Summary graph showing prepulse inhibition for different prepulse stimuli before (control, black) and after (red, $n = 5$ mice) ZX1 infusion. ***f***, Same as in ***e*** but in ZnT3 KO ($p \leq 0.005$, $n = 4$ mice, one-sample *t* tests). For all panels, asterisks indicate significant differences after accounting for multiple comparisons using the Holm-Bonferroni's correction; error bars indicate SEM. Detailed values and staticistcal test are listed in the Materials and Methods.

by suppression of different types of interneurons can lead to enhanced excitation (expected) and enhanced inhibition (paradoxical) in principal neurons. In this study and a previous report on the effects of synaptic zinc on A1 L2/3 PV sound-evoked responses (Anderson et al., 2017), it is evident that synaptic zinc suppresses PV neuron responses to a wide range of sound intensities and frequencies. Therefore, we suggest that synaptic zinc, by suppressing PV sound-evoked responses, might enhance the overall network-mediated inhibition in L2/3 principal neurons and thus sharpen their sound frequency tuning. Although previous studies have suggested that PV neurons modulate the response gain of principal neurons without affecting their tuning properties (Atallah et al., 2012; Wilson et al., 2012; but see Lee et al., 2012), more recent work shows that the effects of PV neurons on the frequency tuning of principal neurons are more complex and depend on factors such as baseline firing rate and nonlinearities imposed by spike threshold and the strength of feedforward network connections (Phillips and Hasenstaub, 2016; Moore et al., 2018). Although the bulk application of ZX1 limits our ability to distinguish cell- from network-specific effects, we propose that the effects of zinc chelation reflect a combination of the direct effects of zinc on principal, PV, and SOM neurons as well as network-level effects on inhibitory and excitatory signaling, all of which contribute to sound frequency tuning. Future experiments are needed to elucidate the precise synaptic effects of zinc on these different cell types as well as how these effects combine in recurrent and feedforward cortical networks to shape A1 sound processing.

Since synaptic zinc is present in telencephalic neurons but not thalamic neurons (Brown and Dyck, 2003), the effects of zinc are likely not on thalamic inputs directly, but rather on corticocortical synapses that refine these thalamocortical inputs. Additional contributing factors to the cell- and synapse-specific, zinc-mediated effects on A1 sound processing may include different amounts of synaptic zinc release at different A1 synapses, differential composition of synaptic NMDAR and AMPAR subunits, and differential engagement of zinc-mediated endocannabinoid signaling (Perez-Rosello et al., 2013; Kalappa and Tzounopoulos, 2017). Moreover, it is possible that loss of ZnT3 may affect glutamatergic signaling in ZnT3 KO mice. ZnT3 colocalizes to the same synaptic vesicles as the synaptic glutamate transporter Vglut1 and increases the glutamate content of glutamatergic vesicles (Salazar et al., 2005). Although synaptic zinc levels in the dorsal cochlear nucleus can be selectively decreased relative to glutamate levels without affecting glutamatergic neurotransmission (Kalappa et al., 2015), future experiments are needed to test whether ZnT3-dependent changes in glutamatergic neurotransmission might contribute to the altered sound-evoked responses of A1 neurons and the sound frequency discrimination acuity in ZnT3 KO mice.

We used a subtractive strategy to unmask the cell-type-specific effects of synaptic zinc on A1 neurons by measuring how the absence of zinc (by infusing ZX1) changes neuronal sound-evoked responses. Future experiments enhancing zinc levels at specific synapses via zinc transporter modulation will be important for addressing more directly the effect of zinc on frequency tuning and frequency discrimination in A1. Additionally, because we used relatively sparsely spaced sound frequencies, it will be important for future work to increase the sampling density of sound frequencies for more detailed measurements of the effects of zinc on receptive field structure – especially for sound frequency regions several octaves away from BF.

We found that the effects of ZX1 on sound-evoked responses and sound frequency discrimination acuity are ZnT3 dependent (Figs. 1*o*,*p*; 5*f*). However, we do not know whether ZX1 has effects on other neuronal properties, such as spontaneous activity, which is crucial for the ability of PV and SOM neurons to inhibit principal neuron sound-evoked responses in A1 (Phillips et al., 2016; Moore et al., 2018). Moreover, it is unclear whether such effects on spontaneous activity would be attributable to tonic, ZnT3-independent zinc (Anderson et al., 2015). Future experiments assessing the effect of synaptic and tonic zinc will address the role of these two pools of zinc on spontaneous activity in A1.

Ethological and translational implications of zinc signaling in cortical sensory processing

Here, we observed effects of synaptic zinc on frequency tuning at sound intensities from 30 to 70 dB SPL. Together with our previous findings on the effects of synaptic zinc on response gain over a wide range of 30–80 dB SPL sound intensities (Anderson et al., 2017), these results reflect the ethological relevance of synaptic zinc signaling in modulating cortical responses to sound. Disruptions of synaptic zinc, either genetically or pharmacologically (Figs. 4, 5), lead to deficits in sound frequency discrimination acuity, suggesting that synaptic zinc fine-tunes auditory processing and enhances auditory acuity. In addition to auditory discrimination deficits, ZnT3 KO mice also display significant impairments in whisker-mediated, fine-texture discrimination (Wu and Dyck, 2018). Although the cellular/molecular mechanisms via which synaptic zinc enhances fine-texture discrimination remain unknown, these and our results further indicate that synaptic zinc plays a general role in fine-tuning sensory processing across sensory modalities.

Fine-tuning of sensory processing is crucial for ethologically relevant processing of the sensory world, and deficits in this neuronal calibration are associated with disorders such as schizophrenia. Here, we report auditory processing deficits caused by the lack of synaptic zinc in mouse auditory cortex that are similar to the deficits found in individuals with schizophrenia. Namely, schizophrenia patients display dramatic impairments in their ability to discriminate sounds of different frequencies (Rabinowicz et al., 2000). These deficits are attributable to auditory cortical dysfunction and impair the phonological processing of language, the intonation of speech that conveys socially relevant information such as sarcasm and emotion, as well as the sensitivity to ongoing auditory events (Javitt and Sweet, 2015). Therefore, it has been hypothesized that altered auditory cortical processing and deficits in pitch matching significantly contribute to the higher-order cognitive impairments associated with schizophrenia (Javitt and Sweet, 2015). Importantly, variants in the chromosome region containing the *ZnT3* gene are associated with schizophrenia, and ZnT3 mRNA and protein levels are significantly reduced in postmortem cortical tissue from female individuals with schizophrenia compared with controls (Perez-Becerril et al., 2016). Although other aspects of schizophrenia-like phenotypes, such as reduced prepulse inhibition, are not affected in ZnT3 KO mice (Cole et al., 2001; Thackray et al., 2016), synaptic zinc signaling in the auditory cortex may still constitute a promising target for advancing our understanding on the etiology of auditory deficits in schizophrenia.

Aging is associated with reductions in the expression of ZnT3 mRNA and protein in the cortices of mice and humans, and reduced ZnT3 expression is much more robust in Alzheimer's patients (Adlard et al., 2010; Whitfield et al., 2014). People suffering from dementia and cognitive impairment also show reduced ZnT3 expression in their prefrontal and parietal cortices (Whitfield et al., 2014, 2015). Since hearing loss and deficits in auditory processing are associated with dementia and Alzheimer's disease, reduced levels of cortical synaptic zinc could provide a mechanistic link between auditory processing deficits and dementia (Lin et al., 2011; Livingston et al., 2017).

References

Adesnik H, Bruns W, Taniguchi H, Huang ZJ, Scanziani M (2012) A neural circuit for spatial summation in visual cortex. Nature 490:226–231. CrossRef Medline

Adlard PA, Parncutt JM, Finkelstein DI, Bush AI (2010) Cognitive loss in zinc transporter-3 knock-out mice: a phenocopy for the synaptic and memory deficits of Alzheimer's disease? J Neurosci 30:1631–1636. CrossRef Medline

Aizenberg M, Geffen MN (2013) Bidirectional effects of aversive learning on perceptual acuity are mediated by the sensory cortex. Nat Neurosci 16:994–996. CrossRef Medline

Aizenberg M, Mwilambwe-Tshilobo L, Briguglio JJ, Natan RG, Geffen MN (2015) Bidirectional regulation of innate and learned behaviors that rely on frequency discrimination by cortical inhibitory neurons. PLoS Biol 13:e1002308. CrossRef Medline

Anderson CT, Radford RJ, Zastrow ML, Zhang DY, Apfel UP, Lippard SJ, Tzounopoulos T (2015) Modulation of extrasynaptic NMDA receptors by synaptic and tonic zinc. Proc Natl Acad Sci U S A 112:E2705–E2714. CrossRef Medline

Anderson CT, Kumar M, Xiong S, Tzounopoulos T (2017) Cell-specific gain modulation by synaptically released zinc in cortical circuits of audition. eLife 6:e29893. CrossRef Medline

Askew C, Intskirveli I, Metherate R (2017) Systemic nicotine increases gain and narrows receptive fields in A1 via integrated cortical and subcortical actions. eNeuro 4:ENEURO.0192-ENEU17.2017. Medline

Atallah BV, Bruns W, Carandini M, Scanziani M (2012) Parvalbumin-expressing interneurons linearly transform cortical responses to visual stimuli. Neuron 73:159–170. CrossRef Medline

Bandyopadhyay S, Shamma SA, Kanold PO (2010) Dichotomy of functional organization in the mouse auditory cortex. Nat Neurosci 13:361–368. CrossRef Medline

Barnstedt O, Keating P, Weissenberger Y, King AJ, Dahmen JC (2015) Functional microarchitecture of the mouse dorsal inferior colliculus revealed through in vivo two-photon calcium imaging. J Neurosci 35:10927–10939. CrossRef Medline

Bizley JK, Nodal FR, Nelken I, King AJ (2005) Functional organization of ferret auditory cortex. Cereb Cortex 15:1637–1653. CrossRef Medline

Brown CE, Dyck RH (2003) An improved method for visualizing the cell bodies of zincergic neurons. J Neurosci Methods 129:41–47. CrossRef Medline

Chen TW, Wardill TJ, Sun Y, Pulver SR, Renninger SL, Baohan A, Schreiter ER, Kerr RA, Orger MB, Jayaraman V, Looger LL, Svoboda K, Kim DS (2013) Ultrasensitive fluorescent proteins for imaging neuronal activity. Nature 499:295–300. CrossRef Medline

Clause A, Nguyen T, Kandler K (2011) An acoustic startle-based method of assessing frequency discrimination in mice. J Neurosci Methods 200:63–67. CrossRef Medline

Cole TB, Wenzel HJ, Kafer KE, Schwartzkroin PA, Palmiter RD (1999) Elimination of zinc from synaptic vesicles in the intact mouse brain by disruption of the ZnT3 gene. Proc Natl Acad Sci U S A 96:1716–1721. CrossRef Medline

Cole TB, Martyanova A, Palmiter RD (2001) Removing zinc from synaptic vesicles does not impair spatial learning, memory, or sensorimotor functions in the mouse. Brain Res 891:253–265. CrossRef Medline

Davis M, Gendelman DS, Tischler MD, Gendelman PM (1982) A primary acoustic startle circuit: lesion and stimulation studies. J Neurosci 2:791–805. CrossRef Medline

Froemke RC, Carcea I, Barker AJ, Yuan K, Seybold BA, Martins AR, Zaika N, Bernstein H, Wachs M, Levis PA, Polley DB, Merzenich MM, Schreiner CE (2013) Long-term modification of cortical synapses improves sensory perception. Nat Neurosci 16:79–88. CrossRef Medline

Guo W, Chambers AR, Darrow KN, Hancock KE, Shinn-Cunningham BG, Polley DB (2012) Robustness of cortical topography across fields, laminae, anesthetic states, and neurophysiological signal types. J Neurosci 32:9159–9172. CrossRef Medline

Guo W, Clause AR, Barth-Maron A, Polley DB (2017) A corticothalamic circuit for dynamic switching between feature detection and discrimination. Neuron 95:180–194.e5. CrossRef Medline

Guo ZV, Hires SA, Li N, O'Connor DH, Komiyama T, Ophir E, Huber D, Bonardi C, Morandell K, Gutnisky D, Peron S, Xu NL, Cox J, Svoboda K (2014) Procedures for behavioral experiments in head-fixed mice. PLoS One 9:e88678. CrossRef Medline

Harris KD, Shepherd GM (2015) The neocortical circuit: themes and variations. Nat Neurosci 18:170–181. CrossRef Medline

Isaacson JS, Scanziani M (2011) How inhibition shapes cortical activity. Neuron 72:231–243. CrossRef Medline

Issa JB, Haeffele BD, Agarwal A, Bergles DE, Young ED, Yue DT (2014) Multiscale optical Ca(2+) imaging of tonal organization in mouse auditory cortex. Neuron 83:944–959. CrossRef Medline

Javitt DC, Sweet RA (2015) Auditory dysfunction in schizophrenia: integrating clinical and basic features. Nat Rev Neurosci 16:535–550. CrossRef Medline

Joshi A, Middleton JW, Anderson CT, Borges K, Suter BA, Shepherd GM, Tzounopoulos T (2015) Cell-specific activity-dependent fractionation of layer 2/3→5B excitatory signaling in mouse auditory cortex. J Neurosci 35:3112–3123. CrossRef Medline

Kalappa BI, Tzounopoulos T (2017) Context-dependent modulation of excitatory synaptic strength by synaptically released zinc. eNeuro 4:ENEURO.0011–17.2017. CrossRef Medline

Kalappa BI, Anderson CT, Goldberg JM, Lippard SJ, Tzounopoulos T (2015) AMPA receptor inhibition by synaptically released zinc. Proc Natl Acad Sci U S A 112:15749–15754. Medline

Kato HK, Gillet SN, Isaacson JS (2015) Flexible sensory representations in auditory cortex driven by behavioral relevance. Neuron 88:1027–1039. CrossRef Medline

Kato HK, Asinof SK, Isaacson JS (2017) Network-level control of frequency tuning in auditory cortex. Neuron 95:412–423.e4. CrossRef Medline

Lee SH, Kwan AC, Zhang S, Phoumthipphavong V, Flannery JG, Masmanidis SC, Taniguchi H, Huang ZJ, Zhang F, Boyden ES, Deisseroth K, Dan Y

(2012) Activation of specific interneurons improves V1 feature selectivity and visual perception. Nature 488:379–383. CrossRef Medline

Levy RB, Reyes AD (2011) Coexistence of lateral and co-tuned inhibitory configurations in cortical networks. PLoS Comput Biol 7:e1002161. CrossRef Medline

Li LY, Li YT, Zhou M, Tao HW, Zhang LI (2013) Intracortical multiplication of thalamocortical signals in mouse auditory cortex. Nat Neurosci 16:1179–1181. CrossRef Medline

Li LY, Ji XY, Liang F, Li YT, Xiao Z, Tao HW, Zhang LI (2014) A feedforward inhibitory circuit mediates lateral refinement of sensory representation in upper layer 2/3 of mouse primary auditory cortex. J Neurosci 34:13670–13683. CrossRef Medline

Li S, Choi V, Tzounopoulos T (2013) Pathogenic plasticity of Kv7.2/3 channel activity is essential for the induction of tinnitus. Proc Natl Acad Sci U S A 110:9980–9985. CrossRef Medline

Lin FR, Metter EJ, O'Brien RJ, Resnick SM, Zonderman AB, Ferrucci L (2011) Hearing loss and incident dementia. Arch Neurol 68:214–220. Medline

Livingston G, Sommerlad A, Orgeta V, Costafreda SG, Huntley J, Ames D, Ballard C, Banerjee S, Burns A, Cohen-Mansfield J, Cooper C, Fox N, Gitlin LN, Howard R, Kales HC, Larson EB, Ritchie K, Rockwood K, Sampson EL, Samus Q, et al. (2017) Dementia prevention, intervention, and care. Lancet 390:2673–2734. CrossRef

McAllister BB, Dyck RH (2017) Zinc transporter 3 (ZnT3) and vesicular zinc in central nervous system function. Neurosci Biobehav Rev 80:329–350. CrossRef Medline

McGinley MJ, David SV, McCormick DA (2015) Cortical membrane potential signature of optimal states for sensory signal detection. Neuron 87:179–192. CrossRef Medline

Meloni EG, Davis M (1998) The dorsal cochlear nucleus contributes to a high intensity component of the acoustic startle reflex in rats. Hear Res 119:69–80. CrossRef Medline

Merzenich MM, Knight PL, Roth GL (1973) Cochleotopic organization of primary auditory cortex in the cat. Brain Res 63:343–346. CrossRef Medline

Moore AK, Wehr M (2013) Parvalbumin-expressing inhibitory interneurons in auditory cortex are well-tuned for frequency. J Neurosci 33:13713–13723. CrossRef Medline

Moore AK, Weible AP, Balmer TS, Trussell LO, Wehr M (2018) Rapid rebalancing of excitation and inhibition by cortical circuitry. Neuron 97:1341–1355.e6. CrossRef Medline

Ozeki H, Finn IM, Schaffer ES, Miller KD, Ferster D (2009) Inhibitory stabilization of the cortical network underlies visual surround suppression. Neuron 62:578–592. CrossRef Medline

Pakan JM, Lowe SC, Dylda E, Keemink SW, Currie SP, Coutts CA, Rochefort NL (2016) Behavioral-state modulation of inhibition is context-dependent and cell type specific in mouse visual cortex. eLife 5:e14985. CrossRef Medline

Pan E, Zhang XA, Huang Z, Krezel A, Zhao M, Tinberg CE, Lippard SJ, McNamara JO (2011) Vesicular zinc promotes presynaptic and inhibits postsynaptic long-term potentiation of mossy fiber-CA3 synapse. Neuron 71:1116–1126. CrossRef Medline

Patel TP, Man K, Firestein BL, Meaney DF (2015) Automated quantification of neuronal networks and single-cell calcium dynamics using calcium imaging. J Neurosci Methods 243:26–38. CrossRef Medline

Paxinos G, Franklin KBJ (2001) The mouse brain in stereotaxic coordinates. San Diego: Academic.

Perez-Becerril C, Morris AG, Mortimer A, McKenna PJ, de Belleroche J (2016) Common variants in the chromosome 2p23 region containing the SLC30A3 (ZnT3) gene are associated with schizophrenia in female but not male individuals in a large collection of European samples. Psychiatry Res 246:335–340. CrossRef Medline

Perez-Rosello T, Anderson CT, Schopfer FJ, Zhao Y, Gilad D, Salvatore SR, Freeman BA, Hershfinkel M, Aizenman E, Tzounopoulos T (2013) Synaptic Zn2+ inhibits neurotransmitter release by promoting endocannabinoid synthesis. J Neurosci 33:9259–9272. CrossRef Medline

Phillips EA, Hasenstaub AR (2016) Asymmetric effects of activating and inactivating cortical interneurons. eLife 5:e18383. CrossRef Medline

Pologruto TA, Sabatini BL, Svoboda K (2003) ScanImage: flexible software for operating laser scanning microscopes. Biomed Eng Online 2:13. Medline

Priebe NJ, Ferster D (2008) Inhibition, spike threshold, and stimulus selectivity in primary visual cortex. Neuron 57:482–497. CrossRef Medline

Rabinowicz EF, Silipo G, Goldman R, Javitt DC (2000) Auditory sensory dysfunction in schizophrenia: imprecision or distractibility? Arch Gen Psychiatry 57:1149–1155. CrossRef Medline

Salazar G, Craige B, Love R, Kalman D, Faundez V (2005) Vglut1 and ZnT3 co-targeting mechanisms regulate vesicular zinc stores in PC12 cells. J Cell Sci 118:1911–1921. CrossRef Medline

Sohoglu E, Chait M (2016) Neural dynamics of change detection in crowded acoustic scenes. Neuroimage 126:164–172. CrossRef Medline

Suter BA, O'Connor T, Iyer V, Petreanu LT, Hooks BM, Kiritani T, Svoboda K, Shepherd GM (2010) Ephus: multipurpose data acquisition software for neuroscience experiments. Front Neural Circuits 4:100. Medline

Thackray SE, McAllister BB, Dyck RH (2016) Behavioral characterization of female zinc transporter 3 (ZnT3) knockout mice. Behav Brain Res 321:36–49. CrossRef Medline

Tremblay R, Lee S, Rudy B (2016) GABAergic interneurons in the neocortex: from cellular properties to circuits. Neuron 91:260–292. CrossRef Medline

Vergnano AM, Rebola N, Savtchenko LP, Pinheiro PS, Casado M, Kieffer BL, Rusakov DA, Mulle C, Paoletti P (2014) Zinc dynamics and action at excitatory synapses. Neuron 82:1101–1114. CrossRef Medline

Vogt K, Mellor J, Tong G, Nicoll R (2000) The actions of synaptically released zinc at hippocampal mossy fiber synapses. Neuron 26:187–196. CrossRef Medline

Wehr M, Zador AM (2003) Balanced inhibition underlies tuning and sharpens spike timing in auditory cortex. Nature 426:442–446. CrossRef Medline

Whitfield DR, Vallortigara J, Alghamdi A, Howlett D, Hortobágyi T, Johnson M, Attems J, Newhouse S, Ballard C, Thomas AJ, O'Brien JT, Aarsland D, Francis PT (2014) Assessment of ZnT3 and PSD95 protein levels in Lewy body dementias and Alzheimer's disease: association with cognitive impairment. Neurobiol Aging 35:2836–2844. CrossRef Medline

Whitfield DR, Vallortigara J, Alghamdi A, Hortobágyi T, Ballard C, Thomas AJ, O'Brien JT, Aarsland D, Francis PT (2015) Depression and synaptic zinc regulation in Alzheimer disease, dementia with Lewy bodies, and Parkinson disease dementia. Am J Geriatr Psychiatry 23:141–148. CrossRef

Wilson NR, Runyan CA, Wang FL, Sur M (2012) Division and subtraction by distinct cortical inhibitory networks in vivo. Nature 488:343–348. CrossRef Medline

Wu GK, Arbuckle R, Liu BH, Tao HW, Zhang LI (2008) Lateral sharpening of cortical frequency tuning by approximately balanced inhibition. Neuron 58:132–143. CrossRef Medline

Wu HP, Dyck R (2018) Signaling by synaptic zinc is required for whisker-mediated, fine texture discrimination. Neuroscience 369:242–247. CrossRef Medline

Zhang LI, Tan AY, Schreiner CE, Merzenich MM (2003) Topography and synaptic shaping of direction selectivity in primary auditory cortex. Nature 424:201–205. CrossRef Medline